General Disclaimer

One or more of the Following Statements may affect this Document

- This document has been reproduced from the best copy furnished by the organizational source. It is being released in the interest of making available as much information as possible.

- This document may contain data, which exceeds the sheet parameters. It was furnished in this condition by the organizational source and is the best copy available.

- This document may contain tone-on-tone or color graphs, charts and/or pictures, which have been reproduced in black and white.

- This document is paginated as submitted by the original source.

- Portions of this document are not fully legible due to the historical nature of some of the material. However, it is the best reproduction available from the original submission.

Magnetic dynamo action in two-dimensional turbulent magneto-hydrodynamics

David Fyfe and Glenn Joyce

Department of Physics and Astronomy, University of Iowa

Iowa City, Iowa 52242

and

David Montgomery*

Advanced Study Program, National Center for Atmospheric Research

Boulder, Colorado 80303

June 1976

*Permanent address: University of Iowa

Abstract

Two-dimensional magnetohydrodynamic turbulence is explored by means of numerical simulation. Previous analytical theory, based on non-dissipative constants of the motion in a truncated Fourier representation, is verified by following the evolution of highly non-equilibrium initial conditions numerically. Dynamo action (conversion of a significant fraction of turbulent kinetic energy into long-wavelength magnetic field energy) is observed. It is conjectured that in the presence of dissipation and external forcing, a dual cascade will be observed for zero-helicity situations. Energy will cascade to higher wave numbers simultaneously with a cascade of mean square vector potential to lower wave numbers, leading to an omni-directional magnetic energy spectrum which varies as $k^{-1/3}$ at lower wave numbers, simultaneously with a buildup of magnetic excitation at the lowest wave number of the system. Equipartition of kinetic and magnetic energies is expected at the highest wave numbers in the system.

1. Introduction

In a variety of diverse situations, a plasma is known to develop magnetic fields on macroscopic spatial scales, with the supporting electric current distributions lying interior to the plasma itself. Several examples will be familiar: (1) "Magnetic dynamo" generation of the earth's magnetic field; (2) protuberances during solar flares whose geometry strongly indicates the motion of magnetic tubes of force; (3) appearance of megagauss magnetic fields when solid targets are irradiated by lasers; (4) "magnetic island" formation in the poloidal magnetic field of a tokamak discharge (though much of this behavior at present is inferred very indirectly); and (5) consolidation of electric current filaments generated from the Weibel instability in relativistic electron beam simulations.

Some of these plasma phenomena seem to have little in common, except for the decision on the part of the plasma in each case to dump a certain fraction of its kinetic energy into the creation of magnetic fields of macroscopic dimensions. The processes by which this happens are generally poorly understood. It is of interest to search for relatively universal mechanisms for generating long-wavelength, self-consistent magnetic fields which do not rely upon solving detailed equations of motion for highly specialized cases. This is particularly true since many, if not all, of the above plasma situations may be highly turbulent.

A precedent for the conversion of microscopic turbulent energy into energy associated with wavelengths comparable in size to the dimensions of the system exists in the theory of two-dimensional Navier-Stokes fluids, in the form of inverse energy cascades. The cascade of energy to ever-shorter wavelengths in three-dimensional Navier-Stokes turbulence is now

widely known, as is the inertial-range $k^{-5/3}$ kinetic energy spectrum which results. Less widely known, but one of the major developments of the last ten years in fluid turbulence theory, is the dual cascade which may result when boundary and/or initial conditions constrain high Reynolds number turbulence to be essentially two-dimensional. (Atmospheric circulation patterns at scales large comparable with the thickness of the earth's atmosphere are an example.) In this case, evidence is accumulating that two quantities are typically cascaded away from any energy source, in opposite directions in wave number space. Enstrophy (mean square vorticity) has a tendency to flow to higher wave numbers, while energy flows to lower wave numbers, thus increasing the degree of long-range organization of the flow. Kolmogoroff dimensional arguments applied to the upper and lower wave number ranges for steady states give characteristic energy spectra of k^{-3} and $k^{-5/3}$, respectively, together with a continual buildup of energy at the longest allowed wavelengths. For analytical, numerical, and experimental discussion of these results, see, e.g., Kraichnan (1967); Leith (1968); Lilly (1969, 1971); Wiin-Nielsen (1967); Pouquet et al. (1975a); and Seyler et al. (1975).

To the extent that the plasmas in the examples treated in the first paragraph of this paper are representable by incompressible magnetohydrodynamic equations, MHD provides a starting point for the dynamo problems described in that paragraph. If in some turbulent situations, magnetic quantities can be shown to cascade naturally to longer wavelengths, these processes will be prime candidates for the development of macroscopic magnetic fields. The mathematical structure employed in the Navier-Stokes case is readily modified to incompressible MHD.

The perception of this possibility appears to have originated with the astrophysics group at the Observatoire de Nice, who have concentrated on the incompressible three-dimensional case (Frisch et al., 1975; Pouquet et al., 1975b; Pouquet and Patterson, 1976). The present calculation being reported here concerns the two-dimensional case, and extends an earlier publication by us (Fyfe and Montgomery, 1975). We have chosen to investigate the two-dimensional case for three reasons: (1) The two- and three-dimensional cases are as different from each other in MHD as in Navier-Stokes theory; (2) suggestions have begun to appear that in strongly-magnetized situations, MHD turbulence becomes two-dimensional with increasing magnetic field strength (Kit and Tsinober, 1971; Schumann, 1976); (3) an inverse magnetic cascade is possible in two dimensions within the framework of a purely isotropic turbulence theory, whereas the three-dimensional case requires the presence of magnetic helicity and thus a departure from isotropy. It is not known to what extent the field variables in the five examples enumerated in the first paragraph are satisfactorily representable by situations in which the fields are independent of one spatial coordinate, though (1) and (5) surely are, and probably others. Finally, external d.c. magnetic fields are easier to include in two dimensions than in three; if they are normal to the plane of variation of the MHD quantities, they do not affect the mathematics at all.

The plan of this manuscript is as follows. Section 2 summarizes the results of the inviscid, infinite-conductivity predictions (Fyfe and Montgomery, 1975). Section 3, which contains the bulk of the new results in this paper, is devoted to the demonstration, by numerical solution of

the equations of motion, of the correctness of the statistical-mechanical predictions of Section 2. Section 4 discusses cascade processes, which necessarily involves the introduction of forcing terms and dissipation (finite transport coefficients). Magnetic energy spectra are predicted. Numerical simulation to verify these predictions, a considerably more ambitious undertaking, is deferred to a third paper in this series.

2. Predictions of the non-dissipative theory; relation to cascades

The first step in discovering a turbulent cascade process can be thought of as identification of the rugged constants of the non-dissipative motion: these, apparently, are the quantities which can be cascaded. What are desired are the integral invariants which result when the dissipative terms are dropped from the governing dynamical equations. By "rugged" constants of the motion, we mean the sub-class of these invariants which are still invariant if both the field variables and the dynamical equations suffer truncation in the form of Fourier series representations with large but finite numbers of terms. In practice, these are all quadratic integrals, and many constants of the motion in the untruncated representations (e.g., the pointwise vorticity in the two-dimensional Navier-Stokes case) are not rugged in this sense.

Constants of the motion once identified can be used to construct thermal equilibrium distributions by the elementary Gibbsian methods of statistical mechanics (Kraichnan, 1975), and one can find canonical ensembles which have exponential dependences on those constants which are "rugged" in the above sense. Multiplying each constant of the motion is its associated reciprocal "temperature," which enters as a Lagrange multiplier when finding the most probable state. Some of these temperatures may be negative, subject only to the overall requirement that the canonical distributions shall be normalizable. From these canonical distributions, such expectation values as mean energies per Fourier mode are calculable in terms of the temperatures by elementary integrations. The temperatures themselves are determined by requiring the expectation values of the rugged invariants to match prescribed initial values for the system at hand.

Once the rugged constants of the motion are established, the reintroduction of dissipation in the system, generally effective only at the shorter wavelengths, is necessary for a cascade process and more generally, for a truly realistic description of the system. If the cascade process is to be seen in its classical, steady-state, Kolmogoroff form, a source of the cascaded quantities, or "forcing term," is required to balance the dissipation. It is assumed that the forcing terms can supply the cascaded quantities at some prescribed rate. Dimensional analysis (or more detailed dynamical arguments) lead to wave number dependences for the spectra of the cascaded quantities.

The program described above requires first of all a knowledge that all the rugged constants of the motion have been identified. This is in some ways the most difficult part of the theory. There is apparently no other way to verify that the constants have all been identified than to solve numerically the dynamical equations in the truncated Fourier representation. The carrying out of this program is the principal content of this paper (see Section 3). In particular, thermal equilibrium modal energy spectra depend strongly upon which constants of the motion are used in the construction of the canonical ensemble. It is of interest, then, to follow the evolution of the dynamical equations from highly non-thermal initial conditions to verify the spectral predictions for the state to which the truncated dynamical equations relax. In Section 4, we shall return to the completion of the Kolmogoroff program for the cascade predictions.

We now summarize the results of the two-dimensional incompressible equilibrium theory (Fyfe and Montgomery, 1975). We consider two-dimensional,

ideal magneto-hydrodynamics in the case in which the field variables have the following geometry in Cartesian coordinates. $\underset{\sim}{B} = (B_x, B_y, 0)$ is the magnetic field; $\underset{\sim}{v} = (v_x, v_y, 0)$ is the fluid velocity; $\underset{\sim}{j} = \nabla \times \underset{\sim}{B} = (0, 0, j_z)$ is the electric current density. $\underset{\sim}{\omega} = \nabla \times \underset{\sim}{v} = (0, 0, \omega_z)$ is the vorticity vector. $\underset{\sim}{a} = (0, 0, a_z)$ is the vector potential, and $\nabla \times \underset{\sim}{a} = \underset{\sim}{B}$. $\underset{\sim}{E} = (0, 0, E_z)$ is the electric field. All quantities are independent of the z coordinate, but depend upon x, y, and the time t. A uniform d.c. magnetic field $\underset{\sim}{B} = (0, 0, B_0)$ can be added at any step of the development without changing the mathematics.

All quantities are Fourier-decomposed assuming periodic boundary conditions over a large square box; e.g.,

$$j_z = \sum_{\underset{\sim}{k}} j(\underset{\sim}{k},t) \exp (i\underset{\sim}{k} \cdot \underset{\sim}{x})$$

$$\omega_z = \sum_{\underset{\sim}{k}} \omega(\underset{\sim}{k},t) \exp (i\underset{\sim}{k} \cdot \underset{\sim}{x}) \qquad (1)$$

and so on. The $\underset{\sim}{k} = (k_x, k_y, 0)$ are summed over all the values $(2\pi/L) \cdot (n_x, n_y, 0)$ where n_x, n_y are any integers for which $n_x^2 + n_y^2 > 0$, and L is the linear dimension of the box.

In the Fourier representation, and in the appropriate dimensionless units, the dynamical equations can be written entirely in terms of $\omega(\underset{\sim}{k},t)$ and $j(\underset{\sim}{k},t)$ (Fyfe and Montgomery, 1975):

$$\frac{\partial \omega(\underset{\sim}{k},t)}{\partial t} = \sum M_1(\underset{\sim}{r},\underset{\sim}{p})\, \delta\, (\underset{\sim}{p} + \underset{\sim}{r} - \underset{\sim}{k})[\omega(\underset{\sim}{r})\omega(\underset{\sim}{p}) - j(\underset{\sim}{r})j(\underset{\sim}{p})] \qquad (2)$$

$$\frac{\partial j(\underset{\sim}{k},t)}{\partial t} = \sum M_2(\underset{\sim}{r},\underset{\sim}{p})\, \delta\, (\underset{\sim}{p} + \underset{\sim}{r} - \underset{\sim}{k})[j(\underset{\sim}{r})\omega(\underset{\sim}{p}) - \omega(\underset{\sim}{r})j(\underset{\sim}{p})] \qquad (3)$$

where the coupling coefficients M_1 and M_2, independent of the field amplitudes, are

$$M_1(\underset{\sim}{r},\underset{\sim}{p}) = M_1(\underset{\sim}{p},\underset{\sim}{r}) = (1/2)\ \hat{e}_z\cdot(\underset{\sim}{r}\times\underset{\sim}{p})\left(\frac{1}{p^2}-\frac{1}{r^2}\right) \tag{4}$$

and

$$M_2(\underset{\sim}{r},\underset{\sim}{p}) = -M_2(\underset{\sim}{p},\underset{\sim}{r}) = (1/2)\ \hat{e}_z\cdot(\underset{\sim}{r}\times\underset{\sim}{p})\ \frac{k^2}{p^2r^2}\ . \tag{5}$$

Here, $\hat{e}_z$ is a unit vector in the z-direction, and $\underset{\sim}{r},\underset{\sim}{p}$ are dummy wave numbers which lie in the xy plane and which are summed over all the values allowed by the periodic boundary conditions. $\delta(\underset{\sim}{p}+\underset{\sim}{r}-\underset{\sim}{k}) = 1$ if $\underset{\sim}{p}+\underset{\sim}{r} = \underset{\sim}{k}$, and is zero otherwise.

Three invariants have been found which survive the restriction of the allowed wave numbers in Eqs. (1), (2), and (3) to lie inside a circular annulus between $|\underset{\sim}{k}| = k_{min}$ and $|\underset{\sim}{k}| = k_{max}$. k_{min} is a minimum wave number determined by the box size, equal to $2\pi/L$, and $k_{max} >> k_{min}$ is a large but finite maximum wave number which, within the framework of the non-dissipative theory, remains physically undetermined. These three invariants are the total energy $\in$, the cross helicity P, and the mean square vector potential A. Referred to unit volume, they are

$$\in \equiv \frac{1}{2}L^{-2}\int dxdy(\underset{\sim}{v}^2+\underset{\sim}{B}^2) = \frac{1}{2}\sum_{\underset{\sim}{k}}\frac{|\omega(\underset{\sim}{k})|^2+|j(\underset{\sim}{k})|^2}{k^2} \tag{6}$$

$$P \equiv \frac{1}{2}L^{-2}\int dxdy\ \underset{\sim}{v}\cdot\underset{\sim}{B} = \frac{1}{2}\sum_{\underset{\sim}{k}}\frac{\omega(\underset{\sim}{k})\ j(-\underset{\sim}{k})}{k^2} \tag{7}$$

$$A \equiv \frac{1}{2} L^{-2} \int dxdy \; \underset{\sim}{a}^2 = \frac{1}{2} \sum_{\underset{\sim}{k}} \frac{|\underset{\sim}{j}(\underset{\sim}{k})|^2}{k^4} \quad . \tag{8}$$

(We have suppressed the time arguments for economy of notation.)

The canonical distribution, in the phase space defined by the real and imaginary parts of the $\underset{\sim}{j}(\underset{\sim}{k})$ and $\omega(\underset{\sim}{k})$, is

$$D = \eta \exp 2(-\alpha \in -\beta ? -\gamma A) \tag{9}$$

where η is a normalizing constant, and $\alpha^{-1}, \beta^{-1}, \gamma^{-1}$ are the energy, helicity, and vector potential temperatures, respectively.

Throughout the balance of this paper, we restrict ourselves to non-helical flows, for which $\langle P \rangle = 0$; from this it can be shown (Fyfe and Montgomery, 1975) that $\beta = 0$. The case of helical flows is deferred to a later publication. Omitting helicity also permits a wholly isotropic formulation of the theory.

For the case of zero helicity, the expectation values calculated from Eq. (9) are

$$\langle |\underset{\sim}{B}(\underset{\sim}{k})|^2 \rangle = (\alpha + \gamma k^{-2})^{-1} \tag{10}$$

and

$$\langle |\underset{\sim}{v}(\underset{\sim}{k})|^2 \rangle = \alpha^{-1} \; . \tag{11}$$

The α and γ are determined as solutions of the pair of simultaneous equations

$$\frac{1}{2} \sum_{\underset{\sim}{k}} \left\{ (\alpha + \gamma\, k^{-2})^{-1} + \alpha^{-1} \right\} = \epsilon \tag{12}$$

and

$$\frac{1}{2} \sum_{\underset{\sim}{k}} (\gamma + k^2 \alpha)^{-1} = A, \tag{13}$$

where ϵ and A are the initial values of the energy and integrated, squared, vector potential for the system under consideration.

More convenient than Eqs. (10) and (11) for numerical investigation are the equivalent spectra for stream function and vector potential given, from Eqs. (10) and (11), by

$$< |\psi(\underset{\sim}{k})|^2 > = \frac{< |v(\underset{\sim}{k})|^2 >}{k^2} = (\alpha k^2)^{-1} \tag{14}$$

and

$$< |a(\underset{\sim}{k})|^2 > = \frac{< |B(\underset{\sim}{k})|^2 >}{k^2} = (\gamma + \alpha k^2)^{-1} \, . \tag{15}$$

α has been shown to be necessarily positive. But γ can either be positive or negative. For fixed ϵ and A, γ always becomes negative if k_{max} is taken large enough. As k_{max} gets larger and larger, $\gamma + \alpha k_{min}^2$ approaches zero, and the vector potential becomes more and more concentrated in the lowest wave number of the system. This is the first and crucial indication of a possible inverse cascade of mean square vector potential.

It should be noted that the sums in Eqs. (6), (7), (8) are over all allowed wave numbers in all four quadrants in $\underset{\sim}{k}$. Not all of these $\underset{\sim}{k}$'s

correspond to independent Fourier coefficients, since the Fourier coefficients in half of the k space determine those in the other half by the reality conditions $\omega(\underset{\sim}{k}) = \omega^*(-\underset{\sim}{k})$ and $j(\underset{\sim}{k}) = j^*(-\underset{\sim}{k})$. For numerical purposes it is more convenient (and equally acceptable) to carry out those sums only over the region $k_x \geq 0$, omitting the modes for which $k_x = 0$ and $k_y < 0$, in Eqs. (6), (7), (8), (12) and (13). That is, we may if we choose sum only over the independent $\underset{\sim}{k}$-modes. This is done in Sec. III.

3. Numerical simulation, and comparison with theory

The dynamical equations are solved by a spectral method closely related to the method of Orszag (1971) and Patterson and Orszag (1971) (see also: Salu and Knorr, 1975 and Seyler et al., 1975). Rather than solving Eqs. (2) and (3), which are more convenient for theoretical purposes, it is preferable numerically to solve the equivalent pair of equations for the vorticity and vector potential,

$$\frac{\partial \omega_z}{\partial t} = -\underset{\sim}{v}\cdot\nabla\omega_z + \underset{\sim}{B}\cdot\nabla j_z \tag{16}$$

$$\frac{\partial a_z}{\partial t} = -\underset{\sim}{v}\cdot\nabla a_z \tag{17}$$

with the various quantities appropriately Fourier-decomposed. All other field quantities are expressible in terms of the solutions tc (16) and (17). It is of the essence of the spectral method that the products on the right hand sides of Eqs. (16) and (17) are evaluated in position space rather than as convolution sums, with a fast Fourier transform back to $\underset{\sim}{k}$-space before the Fourier coefficients are advanced at the next time step (see Patterson and Orszag, 1971 or Salu and Knorr, 1975).

Initial conditions are specified by giving the t = 0 values of the Fourier coefficients. This also facilitates numerical solution of Eqs. '12) and (13) for α and γ. As in our earlier work (Seyler et al., 1975), we choose highly non-thermal initial conditions, by setting all Fourier coefficients initially zero outside a ring in $\underset{\sim}{k}$-space. All excitations then move to both larger and smaller values of $|\underset{\sim}{k}|$ according to the solutions of (16) and (17). Eventually, a state is reached in

which the amplitudes, though still fluctuating with time, show no systematic drift toward either larger or smaller values. We then time-average the squares of the Fourier coefficients over a long enough interval that the average becomes essentially independent of time. The upper limits on the time intervals over which we may average are indicated by the time over which our three constants of the motion ($\mathcal{E}$, A, and $P \equiv 0$) drift away from their initial values. These time averages are then compared with the theoretical predictions of Eqs. (14) and (15).

Several runs were carried out, and we illustrate the results by a description of the two runs to which the greatest amounts of computer time were devoted, and upon which the most diagnostics were performed. One of these, called run F1 hereafter, corresponds to $\gamma < 0$; the other, called run J2 hereafter, corresponds to $\gamma > 0$. Table 1 summarizes the important parameters for these two runs.

Fig. 1 consists of three panels. Fig. 1a shows the initial values of $|a(\underset{\sim}{k})|^2$ vs. k^2 for run F1. Fig. 1b shows the time averages of the $|a(\underset{\sim}{k})|^2$ between times 17.5 and 26.25 for run F1. Fig. 1c shows the time average of the $|a(\underset{\sim}{k})|^2$ between times 35.0 and 52.5, at the end of run F1. The solid curve in Fig. 1c is the theoretical curve, Eq. (15). Different values of $\underset{\sim}{k}$ which correspond to the same value of k^2 have been averaged over in all spectral plots.

Fig. 2 consists also of three panels, which are the corresponding stream function spectra $\psi|(\underset{\sim}{k})|^2$ for run F1. Fig. 2a shows the initial $|\psi(\underset{\sim}{k})|^2$, Fig. 2b shows the time averaged $|\psi(\underset{\sim}{k})|^2$ between times 17.5 and 26.25, and Fig. 2c shows the time averaged $|\psi(\underset{\sim}{k})|^2$ between times 35.0 and 52.5, at the end of the run. The solid curve in Fig. 2c is the theoretical curve, Eq. (14).

Figs. 3 and 4, consisting of three panels each, show the corresponding quantities for run J2. Fig. 3a is the initial data for the $|a(\underset{\sim}{k})|^2$, Fig. 3b is a time average of the $|a(\underset{\sim}{k})|^2$ between times 24.0 and 31.0, and Fig. 3c is the time average of $|a(\underset{\sim}{k})|^2$ between times 34.5 and 51.0, at the end of run J2. The solid line in Fig. 3c is the theoretical curve, Eq. (15). The three panels of Fig. 4 are the corresponding stream function plots ($|\psi(\underset{\sim}{k})|^2$ vs. k^2) for run J2.

Figs. 1 through 4 are considered to be verification of the spectral predictions of the Eqs. (14) and (15), the most important aspects of the non-dissipative equilibrium theory.

Dynamo action (i.e., the conversion of kinetic energy into magnetic energy) is shown in Fig. 5. Fig. 5 is a plot of the ratios of total magnetic energy to total kinetic energy versus time, for both runs. The theoretical predictions are indicated by the arrows on the right hand side of the graph.

The time history of representative modal energies, averaged over modes for a fixed k^2, but differing $\underset{\sim}{k}$, are shown in Fig. 6 for run F1. Fig. 6a shows $|\underset{\sim}{B}(\underset{\sim}{k})|^2$ vs. time for $k^2 = 1, 2, 8,$ and 26. Fig. 6b shows $|\underset{\sim}{v}(\underset{\sim}{k})|^2$ vs. time for the same values of k^2. It is characteristic of the magnetohydrodynamic problem (and is the principal observed difference from the two-dimensional Navier-Stokes case) that the temporal variations of the $|\underset{\sim}{B}(\underset{\sim}{k})|^2$ for low values of $\underset{\sim}{k}$ are significantly slower than the temporal variations of the $|\underset{\sim}{v}(\underset{\sim}{k})|^2$, or of the $|\underset{\sim}{B}(\underset{\sim}{k})|^2$ for higher values of $\underset{\sim}{k}$. This confirms qualitatively an expectation raised by noting that, in Eqs. (2) to (5),

$$\left|\frac{M_2(\underset{\sim}{r},\underset{\sim}{p})}{M_1(\underset{\sim}{r},\underset{\sim}{p})}\right| \longrightarrow 0\left(\frac{k}{2p(\hat{p}\cdot\hat{k})}\right) ,$$

for $k << p$. Thus the flow of magnetic energy to the lowest order modes is expected to be very slow compared to the flow of kinetic energy among the same modes. This can be seen in Fig. 6.

Fig. 7 shows contour plots of constant a_z at four different times in the evolution of run F1. Fig. 8 shows similar contour plots for constant stream function ψ. Fig. 9 shows contour plots of constant a_z at four different times during the evolution of run J2, and Fig. 10 shows the evolution of the stream function ψ for run J2 in the same fashion. Particularly in Fig. 7, it will be seen that the migration of magnetic energy to longer wavelengths is accompanied by the growth and consolidation of the contours of constant a_z (which, in this geometry, are also magnetic field lines). The measure of the total area occupied by any range of a_z values remains, however, approximately constant.

The result has been often quoted, but apparently not proved, that ideal magnetohydrodynamics permits no changes in the topologies of closed magnetic field lines in two-dimensional situations in magnetofluids. We do not know if the result is true, but it should be kept in mind that in any case, the result certainly does not apply to two-dimensional MHD in the truncated Fourier representation. If a proof could be constructed, it would undoubtedly rely on the invariance of the two-dimensional analogue of the Alfven flux invariant,

$$\underset{\sim}{I} = I\,\hat{e}_z = \int_1^2 d\underset{\sim}{\ell} \times \underset{\sim}{B},$$

where $d\underset{\sim}{\ell}$ is a vector element of length along a curve moving with the fluid between end points 1 and 2. While I is invariant for the original ideal MHD equations before Fourier decomposition, it does not survive the restriction of Eqs. (2) and (3) to large but finite numbers of terms. I is, like the pointwise vorticity in the ideal Navier-Stokes case (and like a_z in the ideal two-dimensional MHD case) not a "rugged" invariant in the sense of Sec. II. Therefore, no theorems based on its invariance can apply to the present system. This leaves open, as the question remains open in the Navier-Stokes case, the question of the relation of the truncated system (Eqs. (2) and (3)) to the original system of ideal MHD equations. This is an important unanswered question, though its importance is perhaps diminished by the addition of finite viscosity and resistivity (Sec. IV), which likewise destroy the invariance of I. No mathematical investigation of the ideal incompressible MHD equations carried out so far begins to approach in rigor what would be necessary for a resolution of this question. For example, possible singularities which may develop in the ideal MHD equations in the incompressible case have not been addressed; investigations are still stalled for the case of ideal Navier-Stokes fluids, which are a special case of ideal MHD. For this reason it seems necessary to leave this question open for the time being.

That "magnetic islands" do indeed seem to merge in the present truncated representation can be readily seen by looking at sequences of typical closely (temporally) spaced a_z-contour plots. Some of these are shown in Fig. 11. During the sequence shown in Fig. 11, $\in$ and A vary by only .05% and .01%, respectively, so it is not likely that numerical inaccuracies constitute a "dissipation" which is sufficient to overcome any real or conjectured limitations ideal MHD may place on the merging.

4. Addition of dissipation and forcing; spectral predictions

The presence of finite dissipation and forcing modifies Eqs. (2) and (3) to read

$$\frac{\partial \omega(\underset{\sim}{k},t)}{\partial t} = \sum M_1(\underset{\sim}{r},\underset{\sim}{p})\delta(\underset{\sim}{p}+\underset{\sim}{r}-\underset{\sim}{k})[\omega(\underset{\sim}{r})\omega(\underset{\sim}{p})-j(\underset{\sim}{r})j(\underset{\sim}{p})]$$

$$- \nu k^2 \omega(\underset{\sim}{k},t) + f(\underset{\sim}{k},t) \tag{18}$$

$$\frac{\partial j(\underset{\sim}{k},t)}{\partial t} = \sum M_2(\underset{\sim}{r},\underset{\sim}{p})\delta(\underset{\sim}{p}+\underset{\sim}{r}-\underset{\sim}{k})[j(\underset{\sim}{r})\omega(\underset{\sim}{p})-\omega(\underset{\sim}{r})j(\underset{\sim}{p})]$$

$$- \mu k^2 j(\underset{\sim}{k},t) + g(\underset{\sim}{k},t) \ . \tag{19}$$

In Eqs. (18) and (19), ν is a dimensionless viscosity and μ is a dimensionless resistivity. $f(\underset{\sim}{k},t)$ and $g(\underset{\sim}{k},t)$ are prescribed functions of the time which model external forces (mechanical and/or magnetic) which may act on the system. Numerical investigation of the system (18) and (19) is planned. At present, we are not interested in detailed solutions of (18) and (19), but in generalizing the Kolmogoroff program of dimensional analysis to make predictions about possible cascades of ϵ and A which Eqs. (18) and (19) may imply, when ν and μ are very small but non-zero.

Cascade processes have been considered from two different points of view: the original, relatively simple Kolmogoroff (1941) dimensional arguments, and much more sophisticated dynamical arguments which lead, e.g., to logarithmic corrections (cf. Kraichnan, 1973) and which depend upon detailed properties of the Navier-Stokes equations. At the outset, it seems desirable to stay with the simpler point of view, since little is as yet available in the way of accurate information on the detailed

properties of the MHD turbulent solutions, and since it is as yet unclear what the increased sophistication has added to the Kolmogoroff result.

A natural generalization of Kolmogoroff's program seems to be to construct cascadable quantities per unit mass by dividing extensive rugged invariants by the total mass of the system. There are two of these for this situation, the energy per unit mass and the integrated vector potential per unit mass. We abandon the dimensionless variables at this point, which can obscure the dimensional analysis, and revert to c.g.s. laboratory variables. The quantities to be cascaded are therefore (ρ = mass density)

$$\Pi \equiv \frac{\int\left(\frac{1}{2}\rho \underset{\sim}{v}^2 + \underset{\sim}{B}^2/8\pi\right) dxdy}{\int \rho\, dxdy} \tag{20}$$

$$\Lambda \equiv \frac{\int \underset{\sim}{a}^2\, dxdy}{\int \rho\, dxdy} \tag{21}$$

Π is the total energy per unit mass and has dimensionality L^2T^{-2}, while Λ is the integrated vector potential per unit mass and has dimensions L^4T^{-2}. It is assumed that external sources are capable of supplying Π and Λ to the medium at the rates ϵ per unit time and η per unit time respectively.

First, a decision must be made in any dual-cascade situation as to which quantity will cascade in which direction. We proceed by analogy with the Navier-Stokes case, and assume that the quantity which in the the non-dissipative equilibrium theory can be sharply-peaked at small k is the one which can be cascaded to longer wavelength: namely Λ. It is also reasonable that the cascaded quantity which contains the highest

power of k in its defining expression should be cascaded to higher k, since it is the easier quantity to dissipate. The spectrum (omni-directional spectrum) Λ_k, related to Λ by

$$\int_0^\infty \Lambda_k \, dk = \Lambda \, ,$$

has dimensionality L^5T^{-2}. If Λ_k is assumed to depend only upon η and k in the combination $\eta^\alpha k^\beta$, simple arithmetic shows that

$$\begin{aligned} \alpha &= 2/3 \\ \beta &= -7/3 \, . \end{aligned} \tag{22}$$

The essential content of the second of Eqs. (22) is that the omni-directional magnetic energy spectrum, $2\pi k\langle|\underset{\sim}{B}(k)|^2\rangle$, should vary as $k^{-1/3}$. Of course, eventual pile-up of the magnetic energy at the longest wavelength will excite the lowest modes even above this level, as in the Navier-Stokes case.

Eqs. (22) apply below the input wave numbers characterizing the sources $f(\underset{\sim}{k},t)$ and $g(\underset{\sim}{k},t)$. Above these input wave numbers, similar dimensional arguments predict an omni-directional energy spectrum $\sim k^{-5/3}$. Kraichnan (1965), (see also Pouquet et al., 1975b) has proposed in three dimensions an "Alfvén effect" which inhibits energy transfer at the higher wave numbers and would lead to an omni-directional energy spectrum $\sim k^{-3/2}$ instead of $\sim k^{-5/3}$. Present numerical experiments may find it difficult to distinguish between these two possibilities. In any case, it is our opinion that the question of most interest is the possibility of magnetic excitations at the longest wave numbers rather than the precise value of the exponent at large wave numbers. It is this effect which leads to the dynamo action described here.

5. Discussion

It is considered that two basic contributions are contained in the preceding pages: (1) Verification to a considerable extent of some previous predictions about equilibrium statistics of a truncated Fourier representation of the two dimensional MHD equations; (2) A conjecture concerning the cascade of vector potential to longer wavelengths for the same system in the presence of dissipation and external forcing.

It is important to isolate, also, two or three aspects of the problem that have not been resolved and which require further study. Most important of these (which parallels long-standing problems in Navier-Stokes turbulence theory) is the relation of the original ideal MHD equations to their representation in terms of a large but finite Fourier representation. Experience with other systems of ideal fluid equations for which exact information is available suggests the possibility that singularities may form after finite times for most sets of initial conditions. If this is the case, these singularities will not be visible in any finite Fourier representation. It is also possible that while such singularities might form for the ideal MHD equations, the addition of small but finite dissipation might domesticate them (e.g., Grad, 1975). In this case also, the relation of the truncated Fourier representation might obscure the process to some degree. However, all these objections can be raised in simpler form in connection with Navier-Stokes turbulence, and the fact that they are unanswered there has not altered the fact that virtually everything we know about Navier-Stokes turbulence has come about through truncated Fourier representations. To those who are to some degree familiar with the current status of Navier-Stokes turbulence theory, the above limitations may seem less serious than to those who are not.

Acknowledgments

We are grateful, for valuable and generous comments, to Dr. A. Pouquet, who also derived independently Eqs. (22).

This work was supported in part at the University of Iowa under NASA Grant NGL-16-001-043 and USERDA Grant At(11-1)-2059. The computations were performed in part at the National Center for Atmospheric Research, which is sponsored by the National Science Foundation.

REFERENCES

FRISCH, U., POUQUET, A., LÉORAT, J. & MAZURE, A. 1975 J. Fluid Mech. 68, 769.

FYFE, D. & MONTGOMERY, D. 1975 "High beta turbulence in two-dimensional magnetohydrodynamics." To be published in J. Plasma. Phys.

GRAD, H. 1975 Proc. Nat. Acad. Sci. USA 72, 3789.

KIT, L. G. & TSINOBER, A. B. 1971 Magnitaya Gidrodinamika 3, 27. [English translation: Magnetohydrodynamics 7, 312 (1971)].

KOLMOGOROFF, A. N. 1941 C.R. Acad. Sci. U.S.S.R. 30, 301 and 538.

KRAICHNAN, R. H. 1965 Phys. Fluids 8, 1385.

_____ 1967 Phys. Fluids 10, 1417.

_____ 1973 J. Fluid Mech. 62, 305.

_____ 1975 J. Fluid Mech. 67, 155.

LEITH, C. E. 1968 Phys. Fluids 11, 671.

LILLY, D. K. 1969 Phys. Fluids Suppl. II, 240.

_____ 1971 J. Fluid Mech. 45, 395.

ORSZAG, S. A. 1971 Stud. Appl. Math. 50, 293.

PATTERSON, G. S., JR. &. ORSZAG, S. A. 1971 Phys. Fluids 14, 2358.

POUQUET, A., LESIEUR, M., ANDRE, J. C. & BASDEVANT, C. 1975a J. Fluid Mech. 72, 305.

_____, FRISCH, U. & LÉORAT, J. 1975b "Strong helical turbulence and the nonlinear dynamo effect", Preprint, Observatoire de Nice.

_____ & PATTERSON, G. S., JR. 1976 "Numerical simulation of helical magnetohydrodynamic turbulence." NCAR preprint.

SALU, Y. & KNORR, G. 1975 J. Comp. Phys. 17, 68.

SCHUMANN, U. 1976 J. Fluid Mech. 74, 31.

SEYLER, C. E., JR., SALU, Y., MONTGOMERY, D. & KNORR, G. 1975 Phys. Fluids 18, 803.

WIIN-NIELSEN, A. 1967 Tellus 19, 540.

Table 1

	Run F1	Run J2
Independent $\underset{\sim}{k}$ values for which $\omega(\underset{\sim}{k}) \neq 0$, initially	(3,1),(3,2),(2,3) (3,-1),(3,-2),(2,-3) (1,3)(1,-3)	same as F1
Independent $\underset{\sim}{k}$ values for which $j(\underset{\sim}{k}) \neq 0$, initially	(2,2),(3,0) (0,3),(2,-2)	same as F1
Initial $\mathcal{E}$	4.002	3.962
Initial A	0.125	0.0484
Initial P	zero	zero
α (from initial data)	183.8	179.6
α (from final data)	169.5	169.0
γ (from initial data)	-157.4	92.96
γ (from final data)	-142.0	135.9
Duration of run ($t = t_{max}$)	52.5	52.5
Size of time step (Δt)	$(128)^{-1}$	$(128)^{-1}$
Final $\mathcal{E}$	4.329	4.197
Final A	0.126	0.0490
Final P	0.065	-0.0112
Percent change in $\mathcal{E}$ (at end of run)	8.17	5.93
Percent change in A (at end of run)	0.68	1.23
$k_{min} = 2\pi/L$	1	1
k_{max}	16	16
(Magnetic energy/kinetic energy) Ratio		
Initial	0.361	0.1159
Average over last 2240 time steps	1.047	.9857
Theoretical (from initial data)	1.055	.9873

Figure Captions

Fig. 1 Vector potential spectra $|a(k)|^2$ vs. k^2 for run F1: (a) initial conditions; (b) average over times t = 17.5 to 26.5; (c) average over times 35.0 to 52.5. Theoretical curve is solid line in Fig. 1c. For clarity, only every other value of k^2 is plotted for $50<k^2<100$ and every fourth value for $k^2>100$; the same convention is adopted also in Figs. 2, 3, and 4.

Fig. 2 Stream function spectra $|\psi(k)|^2$ for run F1: (a) initial conditions; (b) average over times 17.5 to 26.5; (c) average over times 35.0 to 52.5. Theoretical curve is solid line in Fig. 2c.

Fig. 3 Vector potential spectra $|a(k)|^2$ vs. k^2 for run J2: (a) initial conditions; (b) average over times 24.0 to 31.0; (c) average over times 34.5 to 51.0. Theoretical curve is solid line in Fig. 3c.

Fig. 4 Stream function spectra $|\psi(k)|^2$ vs. k^2 for run J2: (a) initial conditions; (b) average over times 24.0 to 31.0; (c) average over times 34.5 to 51.0. Theoretical curve is solid line in Fig. 4c.

Fig. 5 Computed ratio of total magnetic energy to total kinetic energy versus time, for runs F1 and J2. Theoretical prediction is indicated at right of graph.

Fig. 6 Time history of energies for fixed k^2 = 1, 2, 8, and 26. (a) $|B(k)|^2$, magnetic energy, and (b) $|v(k)|^2$, kinetic energy. Both are for run F1.

Fig. 7 Contour plots a_z = const at four different times in the evolution of run F1.

Fig. 8 Contour plots ψ = const for stream function at four different times for run F1.

Fig. 9 Contour plots a_z = const at four different times during the evolution of run J2.

Fig. 10 Contour plots ψ = const at four different times during the evolution of run J2.

Fig. 11 Four contour plots a_z = const for run F1 at closely spaced times showing growth and consolidation of magnetic contours, characteristic of $\gamma<0$.

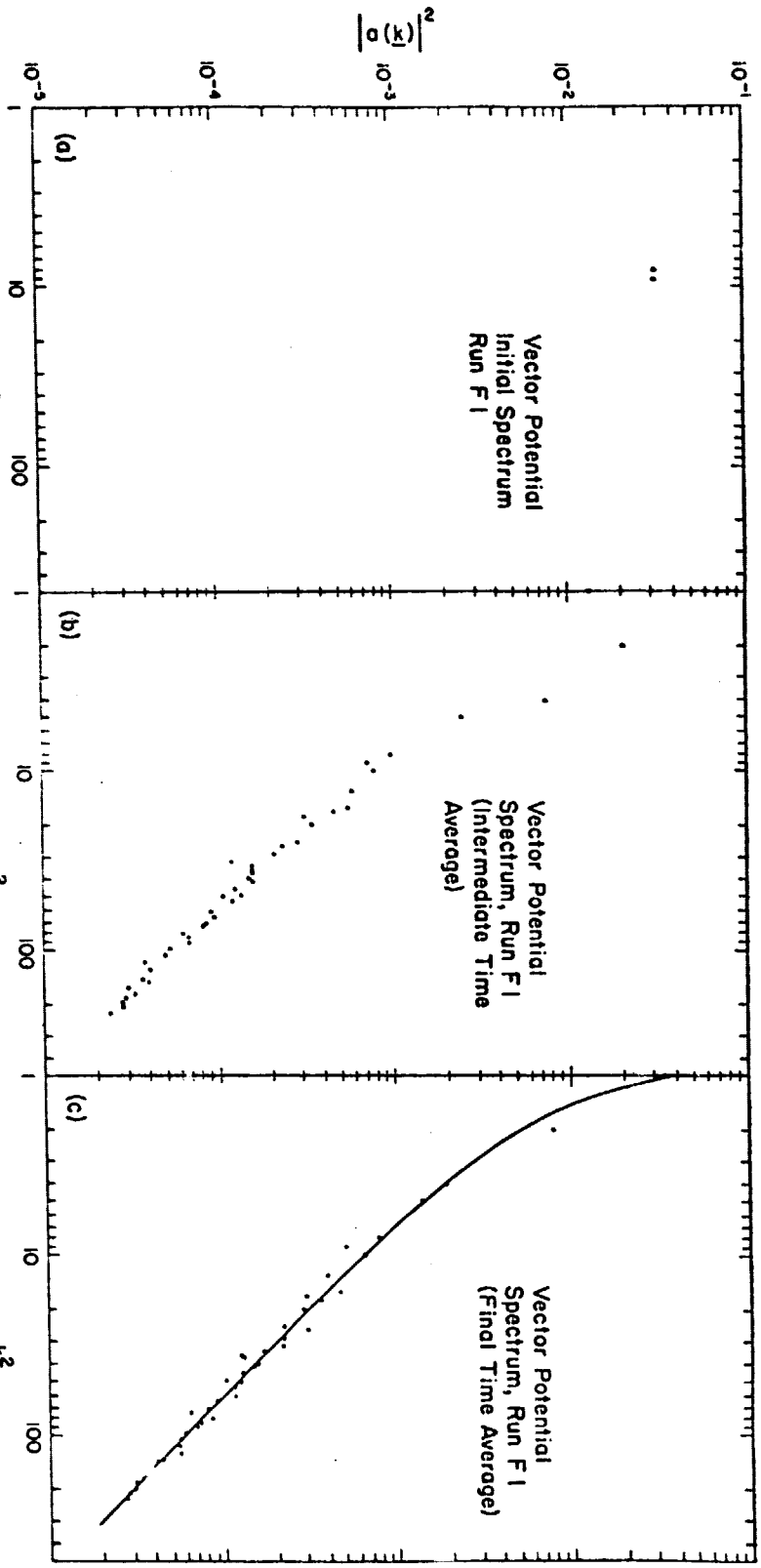

Figures 1a, b, c

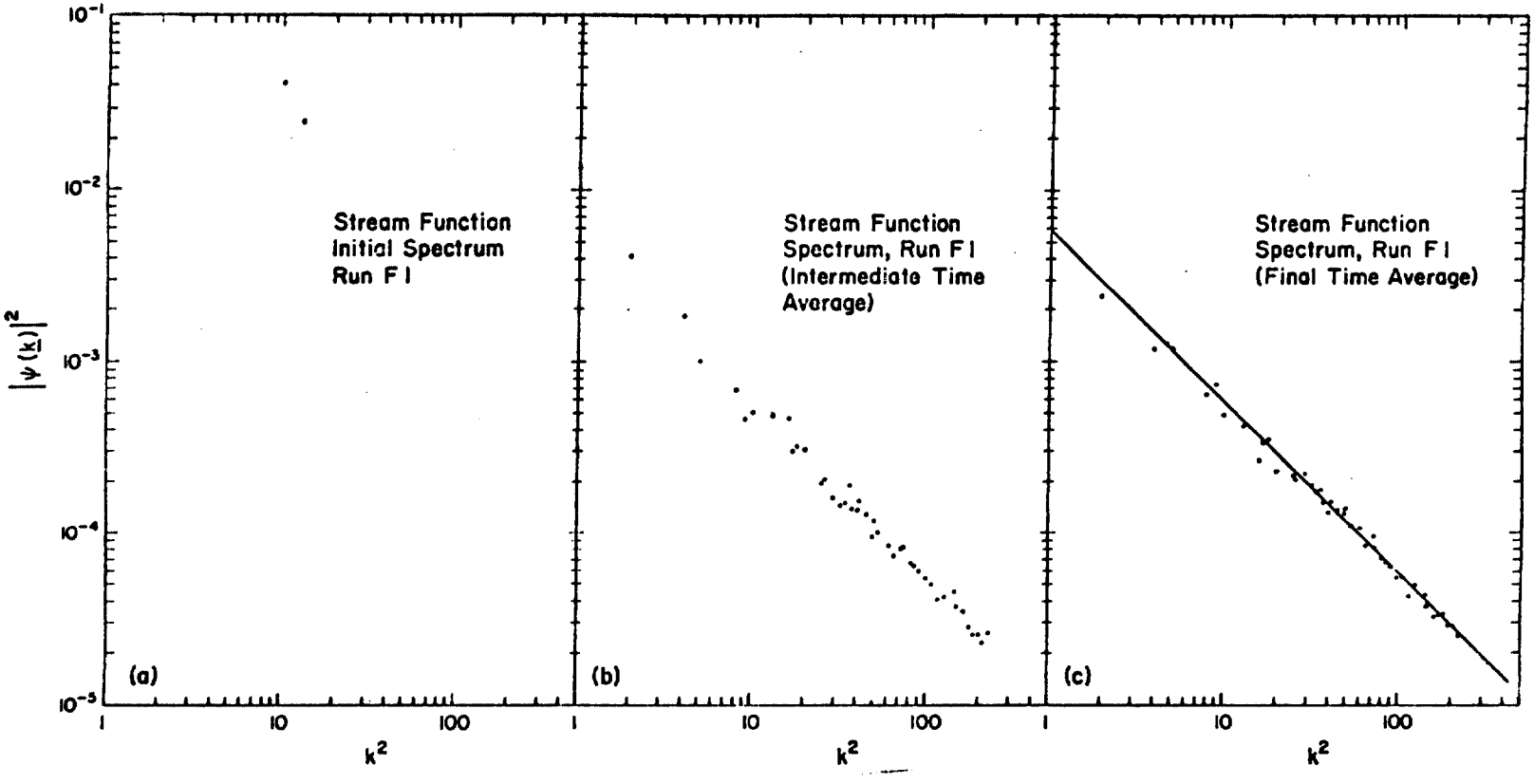

Figures 2a, b, c

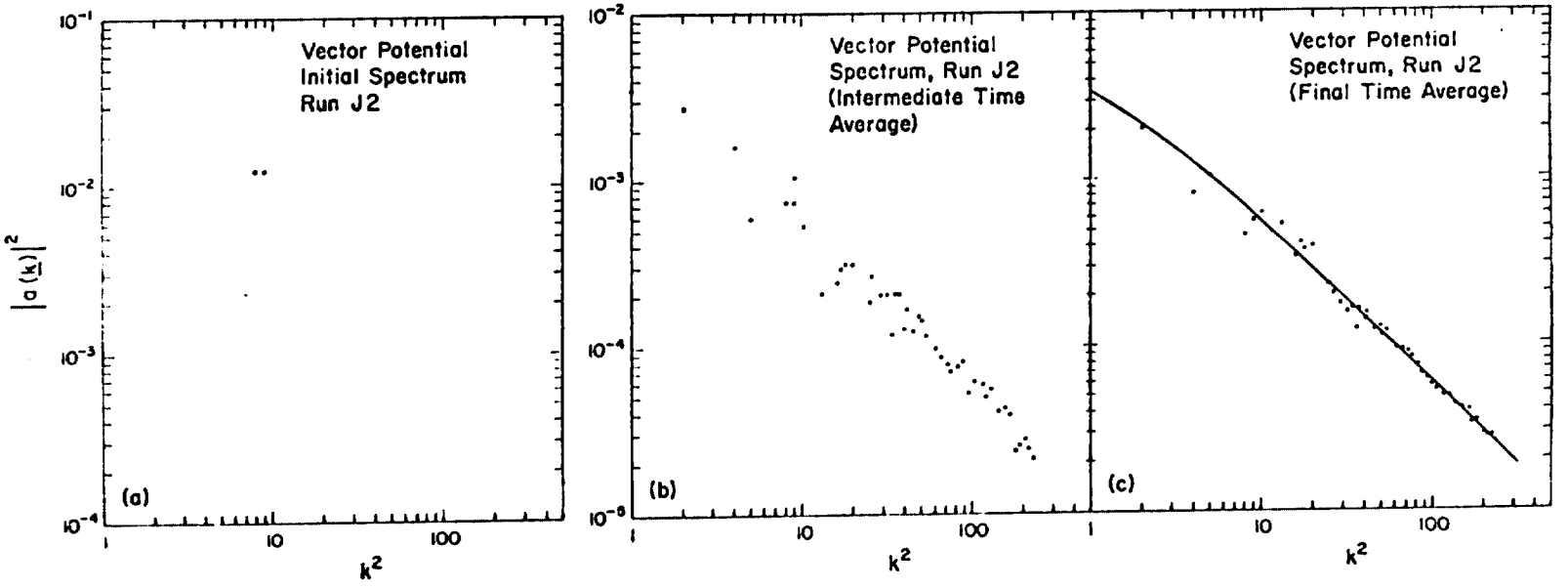

Figures 3a, b, c

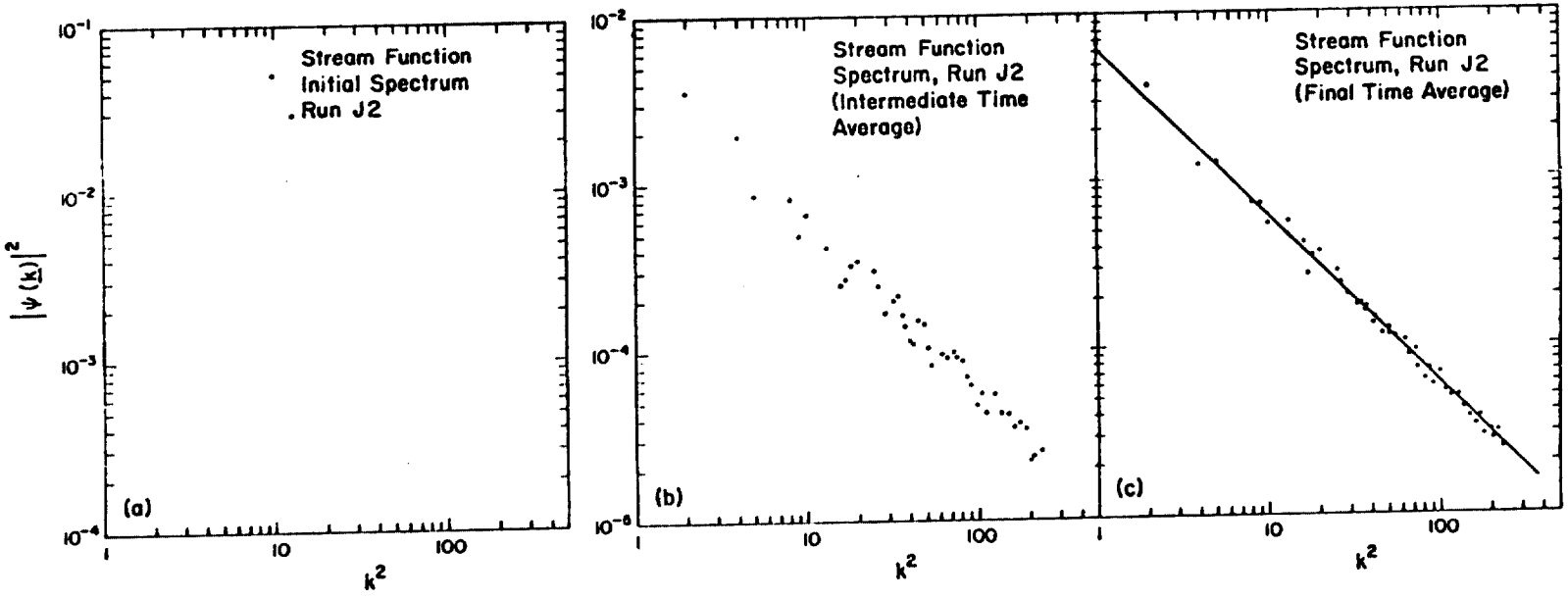

Figures 4a, b, c

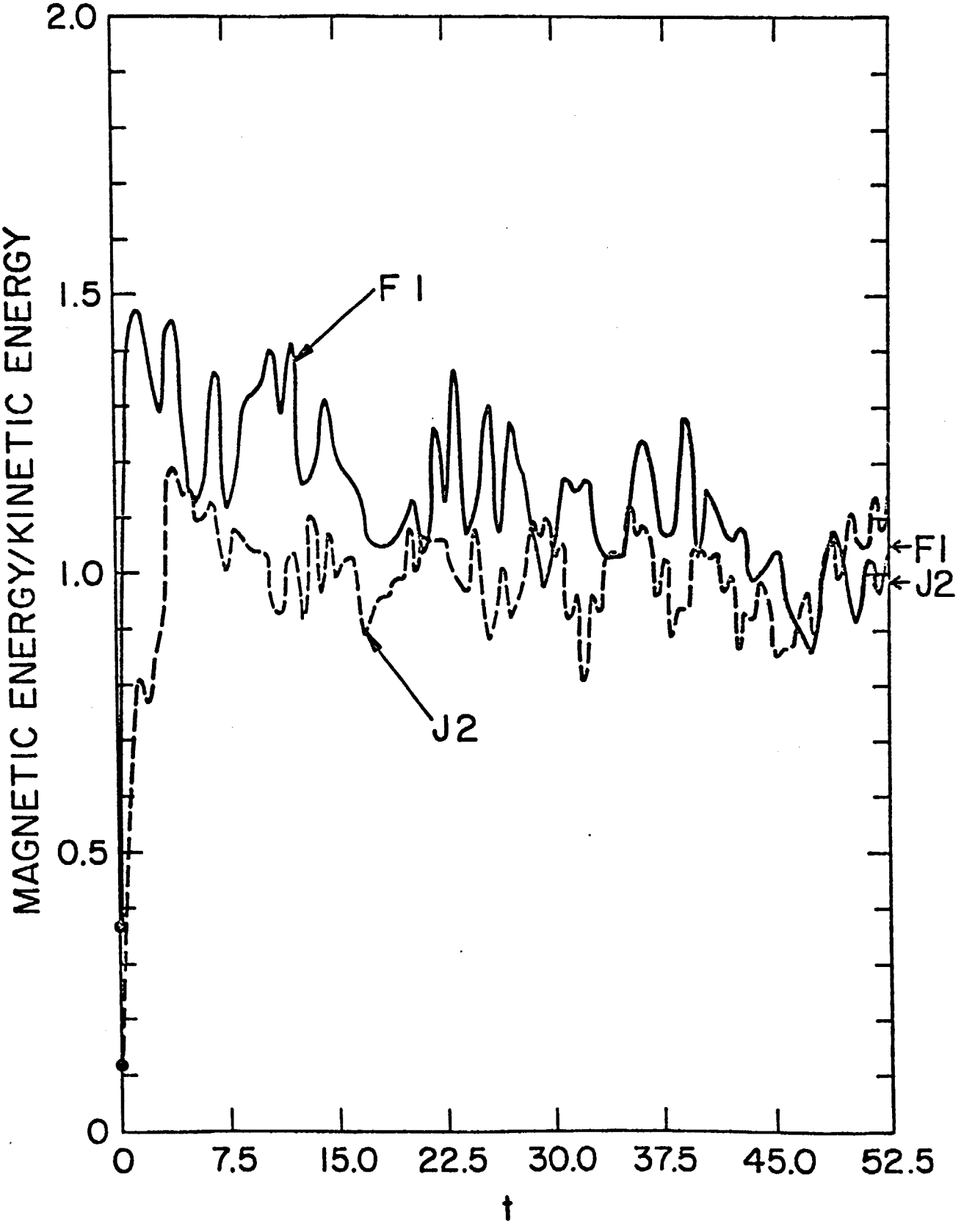
2.0
1.5
1.0
0.5
0
MAGNETIC ENERGY/KINETIC ENERGY
F 1
J2
F1
J2
0
7.5
15.0
22.5
30.0
37.5
45.0
52.5
t

Figure 5

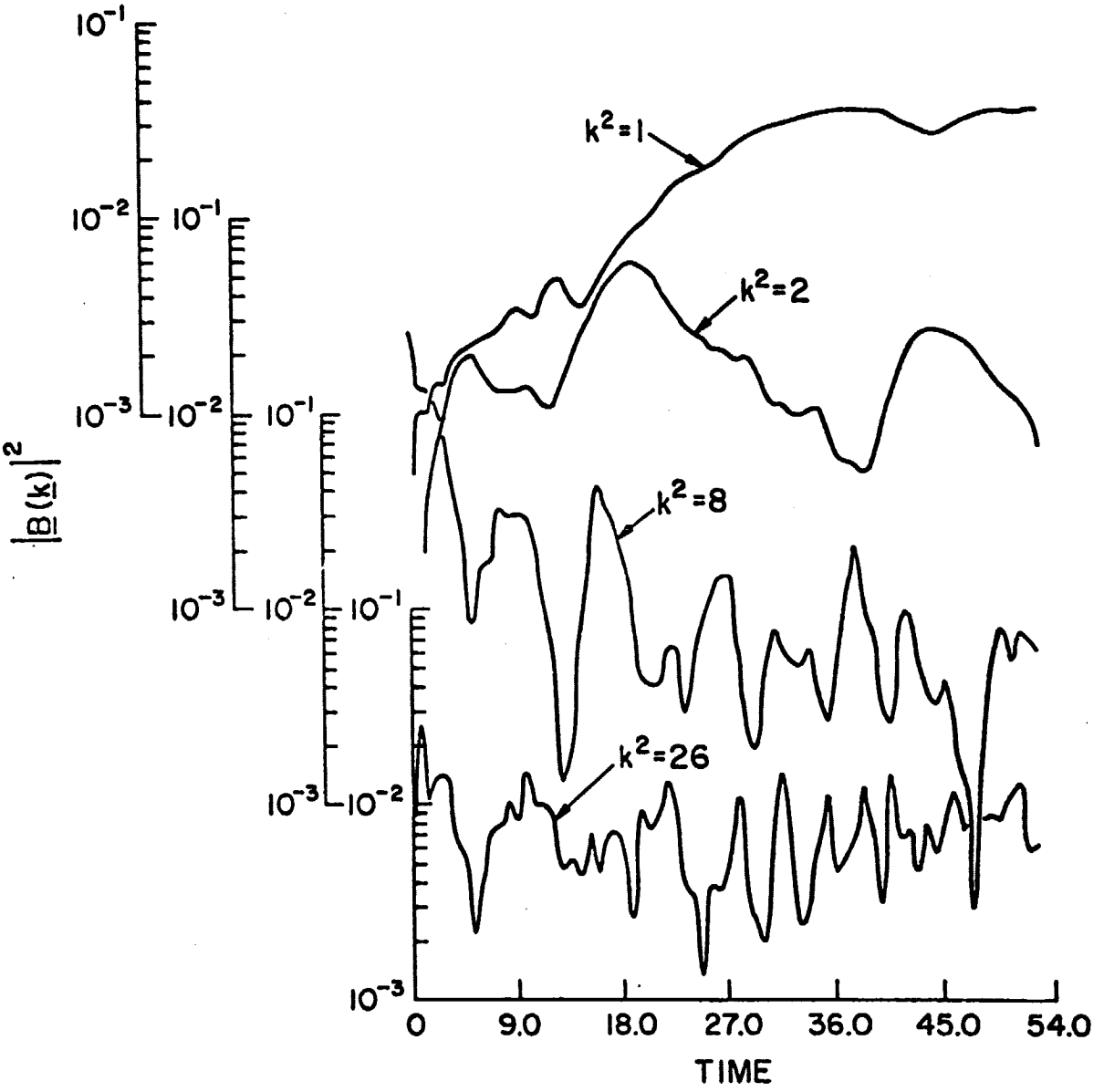
10^{-1}
10^{-2}
10^{-3}
$|\underline{B}(\underline{k})|^2$
$k^2=1$
$k^2=2$
$k^2=8$
$k^2=26$
0
9.0
18.0
27.0
36.0
45.0
54.0
TIME

Figure 6a

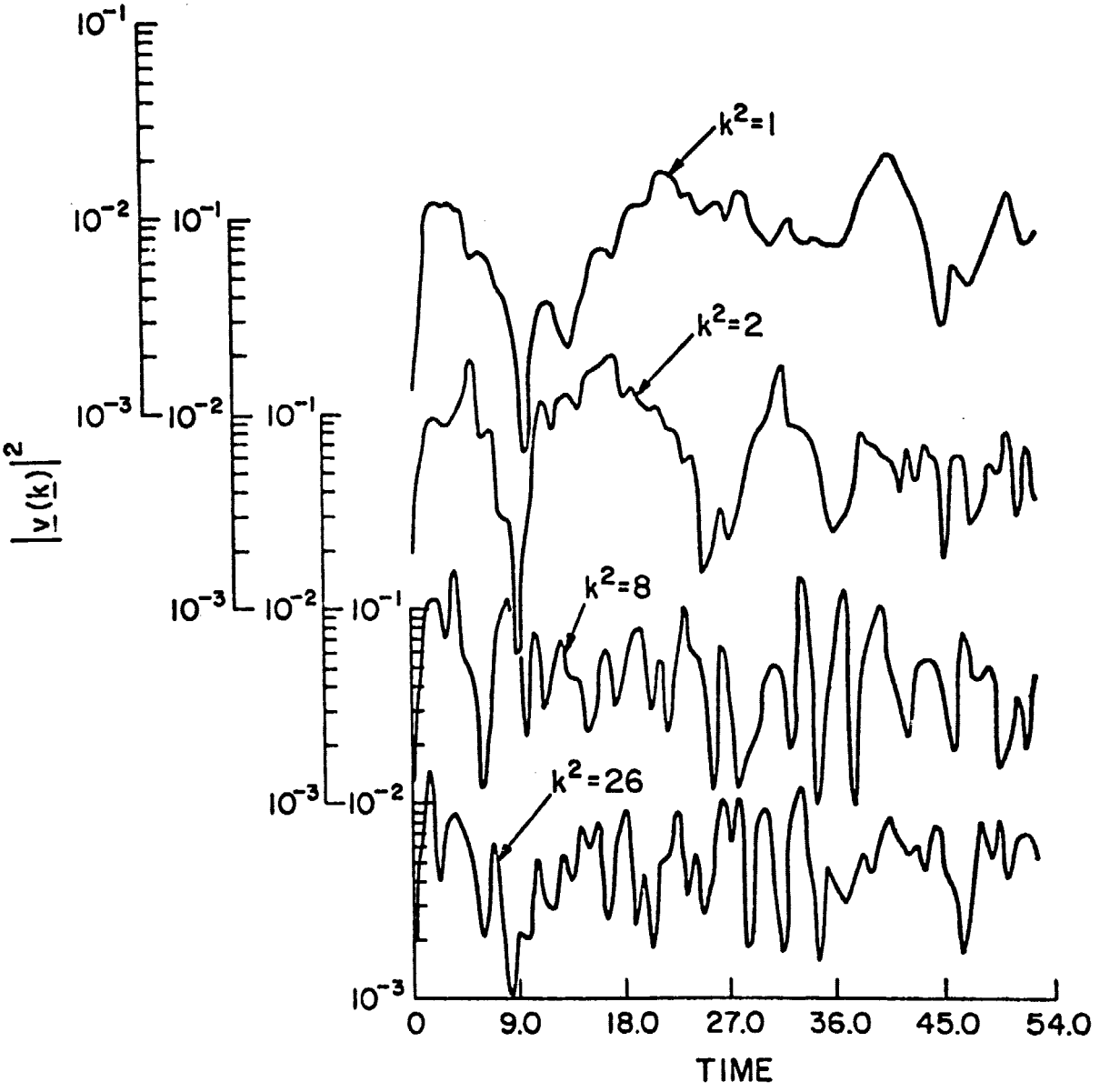

Figure 6b

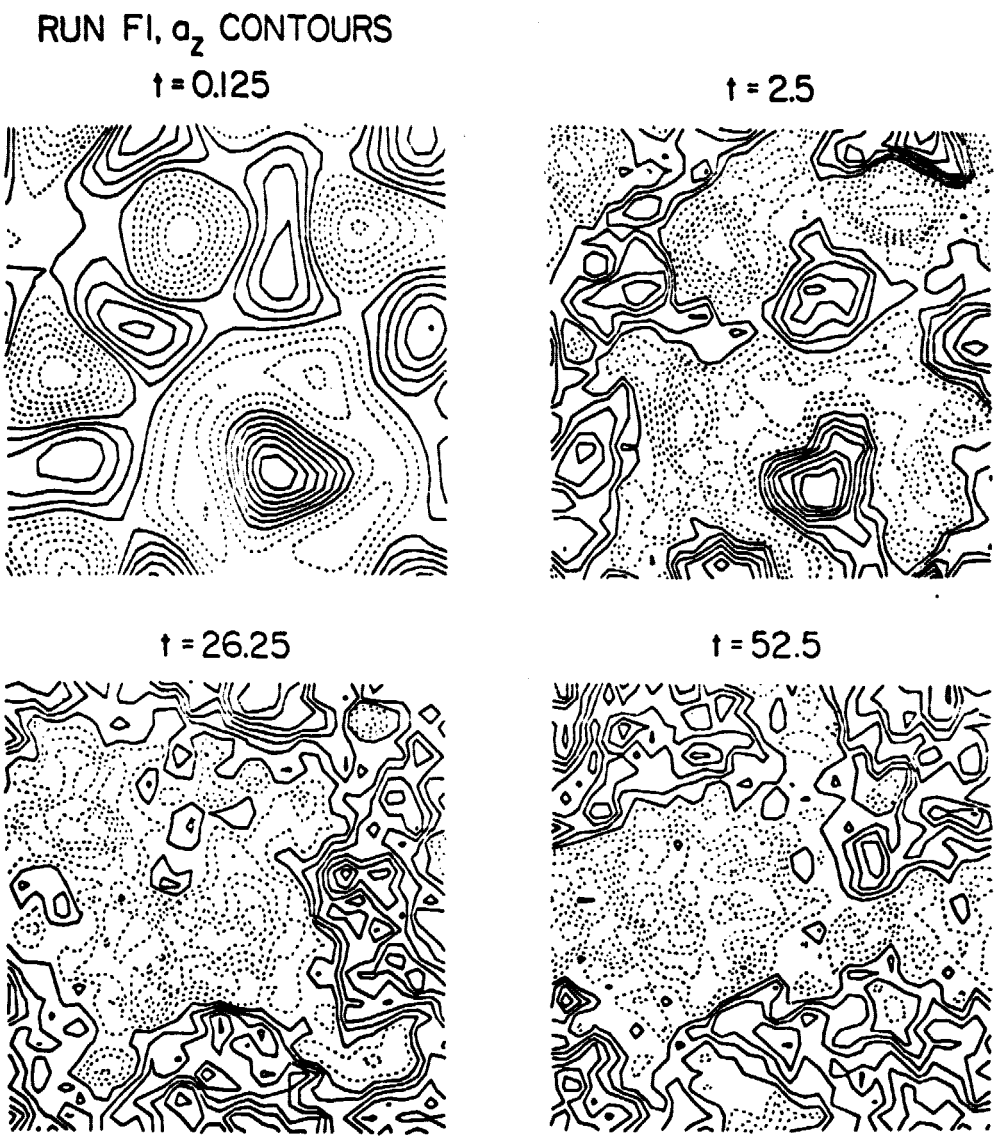

Figure 7

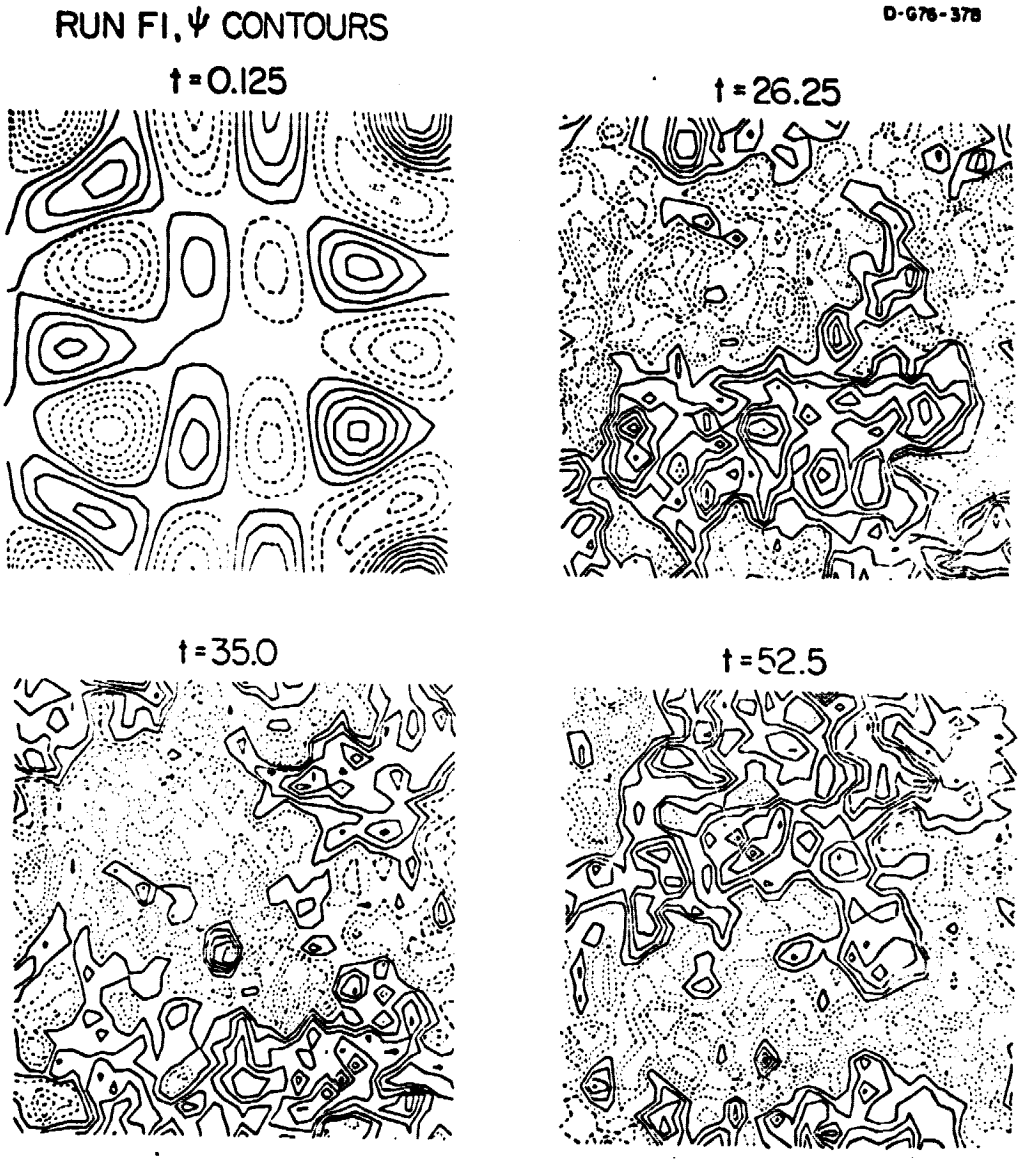

Figure 8

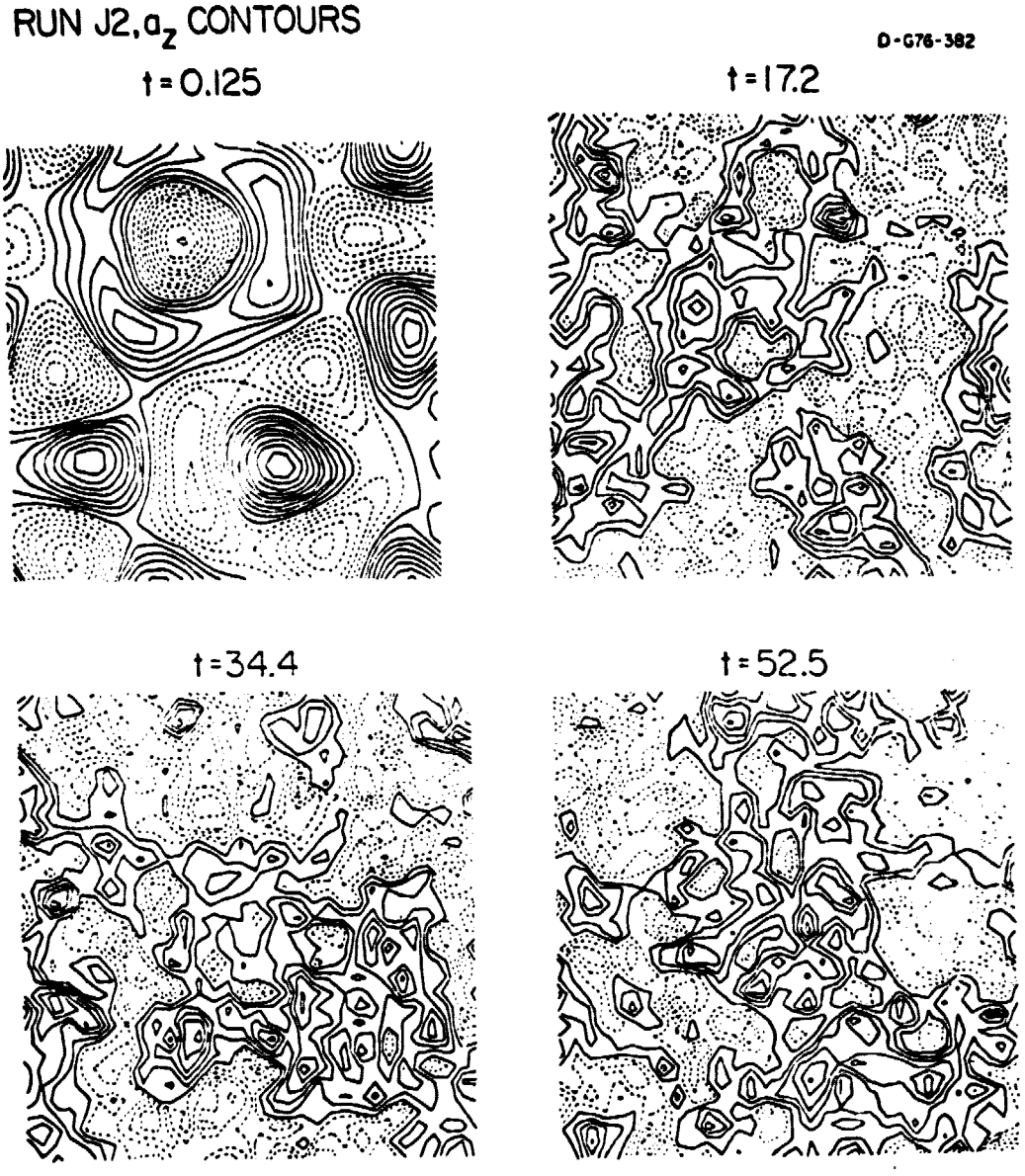

Figure 9

RUN J2, Ψ CONTOURS

D-G76-379

t = 0.125

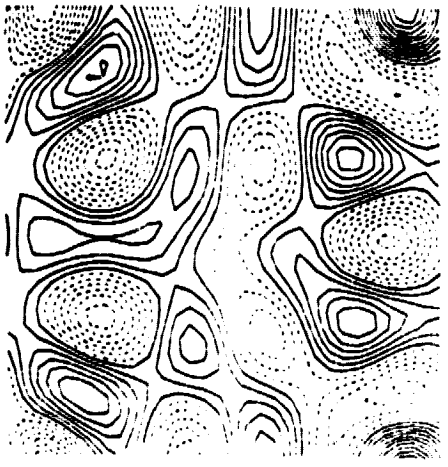

t = 17.2

t = 34.4

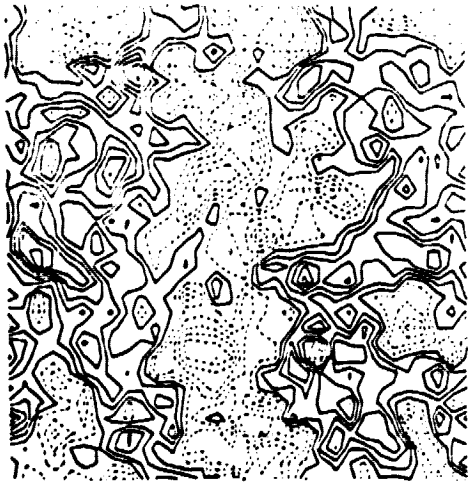

t = 52.5

Figure 10

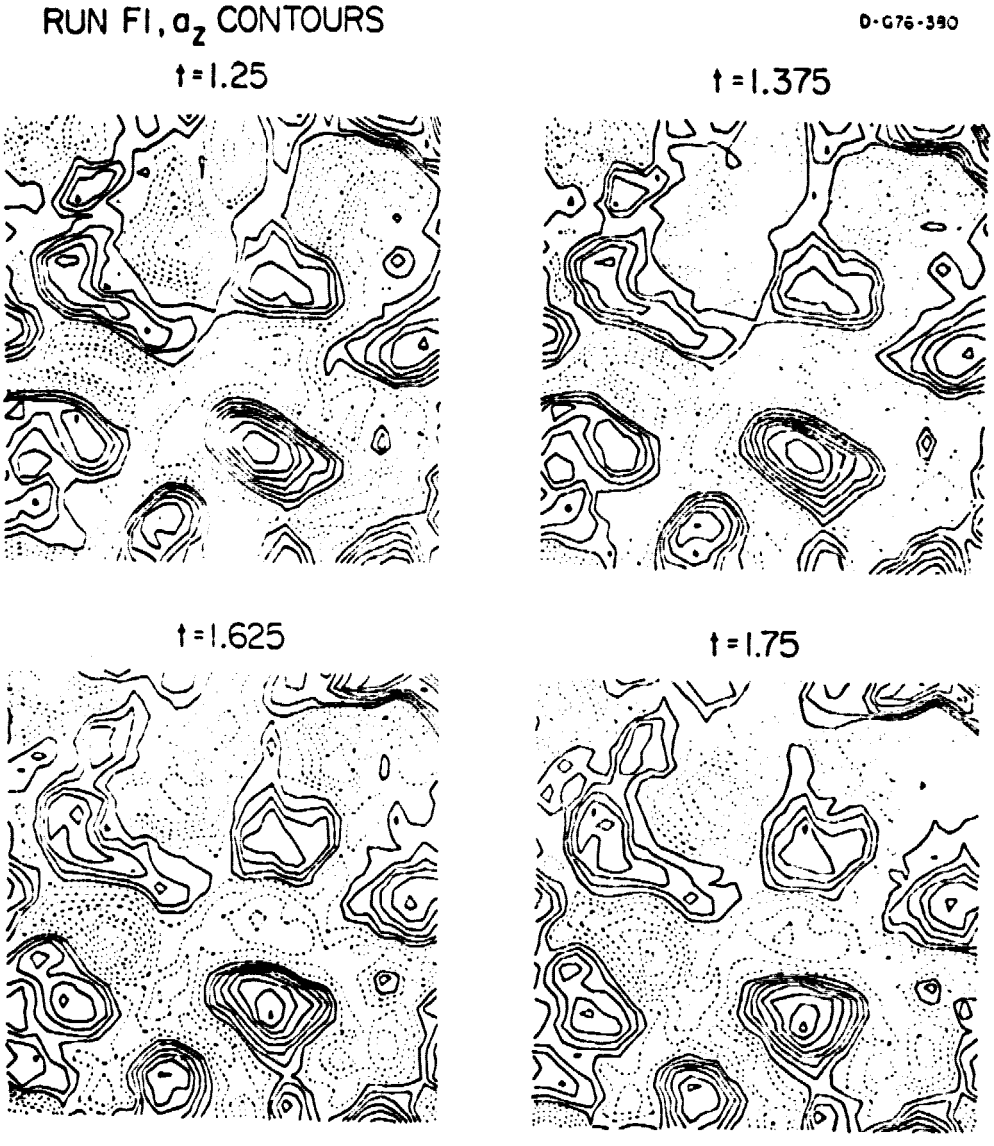

Figure 11